

The Planck Surveyor mission: astrophysical prospects

Gianfranco De Zotti^{*}, Luigi Toffolatti^{*†}, Francisco Argüeso[◇], Rodney D. Davies[‡], Pasquale Mazzotta^{**}, R. Bruce Partridge[○], George F. Smoot^{*}, and Nicola Vittorio^{**}

^{*}*Osservatorio Astronomico di Padova, Vicolo dell'Osservatorio 5, I-35122 Padova, Italy*

[†]*Dep. de Física, Universidad de Oviedo, c.le Calvo Sotelo s/n, E-33007 Oviedo, Spain*

[◇]*Dep. de Matemáticas, Universidad de Oviedo, c.le Calvo Sotelo s/n, E-33007 Oviedo, Spain*

[‡]*Nuffield Radio Astron. Lab., Univ. of Manchester, Jodrell Bank, Macclesfield Cheshire SK11 9DL, UK*

^{*}*LBNL, SSL, Physics Department, University of California, Berkeley, CA 94720, USA*

^{**}*Università di Roma "Tor Vergata", Via della Ricerca Scientifica 1, I-00133 Roma, Italy*

[○]*Haverford College, Haverford, PA 19041-1392, USA*

Abstract.

Although the Planck Surveyor mission is optimized to map the cosmic microwave background anisotropies, it will also provide extremely valuable information on astrophysical phenomena. We review our present understanding of Galactic and extragalactic foregrounds relevant to the mission and discuss on one side, Planck's impact on the study of their properties and, on the other side, to what extent foreground contamination may affect Planck's ability to accurately determine cosmological parameters. Planck's multifrequency surveys will be unique in their coverage of large areas of the sky (actually, of the full sky); this will extend by two or more orders of magnitude the flux density interval over which mm/sub-mm counts of extragalactic sources can be determined by instruments already available (like SCUBA) or planned for the next decade (like the LSA-MMA or the space mission FIRST), which go much deeper but over very limited areas. Planck will thus provide essential complementary information on the epoch-dependent luminosity functions. Bright radio sources will be studied over a poorly explored frequency range where spectral signatures, essential to understand the physical processes that are going on, show up. The Sunyaev-Zeldovich effect, with its extremely rich information content, will be observed in the direction of a large number of rich clusters of Galaxies. Thanks again to its all sky coverage, Planck will provide unique information on the structure and on the emission properties of the interstellar medium in the Galaxy. At the same time, the foregrounds are unlikely to substantially limit Planck's ability to measure the cosmological signals. Even measurements of polarization of the primordial Cosmic Microwave background fluctuations appear to be feasible.

INTRODUCTION

The basic scientific goal of the Planck Surveyor mission is to measure the cosmic microwave background (CMB) anisotropies at all angular scales larger than $5'$, with an accuracy set by astrophysical limits. The mission will produce all-sky maps in 9 frequency bands centered at 30, 44, 70, 100, 143, 217, 353, 545, and 857 GHz, with high sensitivity to intensity fluctuations as well as to polarization fluctuations, accurate calibration (through the modulation of the ~ 3 mK CMB dipole by the orbital motion of the Earth), and a careful minimization of systematic errors. The wide frequency coverage is achieved with two types of detectors: tuned radio receivers at low frequencies (30 to 100 GHz: Low Frequency Instrument or LFI), and bolometers at high frequencies (100 to 857 GHz: High Frequency Instrument or HFI); the 100 GHz band is common to both instruments.

The selected frequency range corresponds to a "cosmological window", where foreground emissions are minimum, while the CMB intensity peaks. At high galactic latitudes CMB intensity fluctuations stand out well above any other astrophysical signal; only in a tiny fraction of pixels in Planck's high Galactic latitude maps, will the cosmological signal be severely contaminated. There are also good prospects for CMB polarization measurements, especially in regions around the ecliptic polar caps, where sensitivities significantly above average are reached.

On the other hand, in spite of the small telescope size, resulting in a low sensitivity to astrophysical sources compared to ground based instruments such as the Effelsberg and Green Bank 100 m telescopes, the VLA, SCUBA on the JCMT, and the mm and sub-mm arrays planned for the next decade, as well as to space-based missions such as FIRST, the Planck surveys will provide unique information on a broad variety of astrophysical phenomena, including synchrotron, free-free and dust emission in our own Galaxy, emissions from several classes of Galactic and extragalactic sources, the Sunyaev-Zeldovich effect in clusters of Galaxies.

FOREGROUNDS AT THE PLANCK SURVEYOR FREQUENCIES

The Galaxy

There are three diffuse Galactic emissions – synchrotron, free-free, and dust – which provide a significant confusing foreground to CMB anisotropy observations. A sketch of the contribution of these components to rms fluctuations at $|b| > 30^\circ$ is shown as a function of frequency by [68]; at high galactic latitudes, the anisotropy in Galactic emission was found to reach a minimum between 50 and 90 GHz.

Particularly at low Galactic latitudes the synchrotron and free-free emissions are recognized as individual radio sources mostly associated with recent star formation: supernova remnants and HII regions, respectively.

Synchrotron emission

Synchrotron emission results from cosmic-ray electrons accelerated in magnetic fields, and thus depends on the energy spectrum of the electrons and the intensity of the magnetic field [102,77]. A recent, careful discussion of the synchrotron emission from the Galaxy has been presented by [27].

If the electrons' direction of motion is random with respect to the magnetic field, and the electrons' energy spectrum can be approximated as a power law: $dN/dE = N_0 E^{-p}$, then the luminosity is given by

$$I(\nu) \propto L N_0 B_{\text{eff}}^{(p+1)/2} \nu^{-(p-1)/2} a(p), \quad (1)$$

where $a(p)$ is a weak function of the electron energy spectrum [77], L is the length along the line of sight through the emitting volume, B is the magnetic field strength, and ν is the frequency.

At GeV energies, the local energy spectrum of the electrons has been measured to be, for the energy intervals describing the peak of radio synchrotron emission, a power law to good approximation. The index of the power law appears to increase from about 2.7 to 3.3 over this energy range [119,87]. Such an increase of the electron energy spectrum slope is expected, as the energy loss mechanisms for electrons increases rapidly (as the square) with energy.

The synchrotron emission at frequency ν is dominated by cosmic ray electrons of energy $E \approx 3(\nu/\text{GHz})^{1/2}$ GeV. The observed steepening of the electrons' spectrum at GeV energies is used to model the radio emission spectrum at GHz frequencies [8].

Radio surveys at frequencies less than 2 GHz are dominated by synchrotron emission. The well-known survey by Haslam et al. [54] at 408 MHz is the only all-sky map available. Large-area surveys with careful attention to baselines and calibration have also been made at 1420 MHz [96] and most recently at 2326 MHz [63]. All these investigations have been made with FWHP beamwidths of less than 1° . Of particular interest for the Planck mission are surveys of significant areas of the sky at higher frequencies, say 5-15 GHz. Only limited data close to the Galactic plane or in selected areas at higher latitudes with restricted angular resolution are available. Surveys of about one steradian of the sky have been made at 5 GHz by [82] at Jodrell Bank and at 10, 15 and 33 GHz by [51] with the Tenerife experiments.

Large features with a synchrotron spectrum extend far from the Galactic plane. The most prominent of these are the spurs and loops which describe small circles on the sky with diameters in the range 60° to 120° [12]. Because of their association with HI and in some cases with X-ray emission, they are believed to be low surface brightness counterparts of the brighter supernova remnants seen in lower latitude surveys such as that by [35] at 2.4 GHz. Other more diffuse structure at higher latitudes may be even older remnants.

The spectral index of Galactic synchrotron emission can be readily determined at frequencies less than 1 GHz where the observational baselevel uncertainty is much less than the total Galactic emission. Lawson et al. [72] used data covering the range 38 to 1420 MHz to determine the spectral index variation over the northern

sky. Clear variations in spectral index of at least 0.3 were found. A steepening in the spectral index at higher frequencies is observed in the brighter features such as the loops and some SNRs. Up to 1420 MHz no such steepening was found in the regions of weaker emission. At the higher Galactic latitudes where no reliable zero level is available at 1420 MHz, an estimate can be made of the spectral index of local features by using the T-T technique. The de-striped 408 and 1420 MHz maps gave temperature spectral indices of 2.8 to 3.2 in the northern galactic pole regions [26].

At frequencies higher than 2-3 GHz no reliable zero levels have been measured for large area surveys. The relevant observational material comes from beamswitching or interferometric data. Accordingly the spectrum of individual features is estimated. On scales of a few degrees the temperature spectral index between 5 GHz [82] and 408 MHz was ~ 3.0 . Similarly the 10, 15 and 33 GHz beam switching data [53] also indicated a spectral index of ~ 3.0 at 10 GHz. These results show that at higher Galactic latitudes synchrotron emission dominates up to 5 GHz and most likely to 10 GHz.

Platania et al. [91] used high frequency data from a number of sky locations to investigate the frequency dependence of the synchrotron emission spectral index and also find evidence for a steepening. Based on the local cosmic ray electron energy spectrum, the synchrotron spectrum should steepen with frequency to about 3.1 at these higher microwave frequencies.

Free-free emission

The Galactic free-free emission (see [110,9] for reviews) is the thermal bremsstrahlung from hot ($\gtrsim 10^4$ K) electrons produced in the interstellar gas by the UV radiation field. This emission is not easily indentified at radio frequencies, except near the Galactic plane. At higher latitudes it must be separated from synchrotron emission by virtue of their different spectral indices. At frequencies less than about 1 GHz, synchrotron emission dominates at intermediate and high latitudes. At higher frequencies where free-free emission might be expected to exceed the synchrotron component, the signals are weak and survey zero levels are indeterminate.

latitudes Diffuse Galactic H α is thought to be a good tracer of diffuse free-free emission since both are emitted by the same ionized medium and both have intensities proportional to emission measure ($\propto EM \equiv \int N_e^2 dl$), the line of sight integral of the free electron density squared. Unfortunately, no full sky map in H α is presently available. Observations of limited areas of the sky have been carried out with a Fabry-Perot spectrometer [98,99,79] or with narrow band filters [45,107]. Note that H α maps are contaminated by a strong geocoronal emission in the same line and by the OH night-sky line at 6568.78 Å. High resolution spectroscopy is required to separate the Galactic H α emission from the contaminating lines, taking advantage of the separation produced by the Doppler shift due to the Earth's motion; the separation, however, is negligible near the ecliptic poles.

The major H α structures form the well-known Local (Gould Belt) System which extends 30°-40° from the plane at positive b in the Galactic centre and at negative latitude in the anticentre. The HI and dust in the Local System may be traced to 50° from the Galactic plane. Other H α features are also found extending 15°-20° from the plane [108]. A substantial H α emission is observed from the Magellanic Stream [121].

To first order, the H α may be modelled as a layer parallel to the Galactic plane with a half-thickness intensity of 1.2 Rayleigh (R). The rms variation in this H α emission is about 0.6 R on degree scales. In the context of the present discussion 1 R ($\equiv 10^6/4\pi$ photons cm $^{-2}$ s $^{-1}$ sr $^{-1}$ = 2.42×10^{-7} erg cm $^{-2}$ sr $^{-1}$ s $^{-1}$ at a wavelength $\lambda_{H\alpha} = 6563$ Å) will give a brightness temperature of about 10 μ K at 45 GHz.

The situation is improving rapidly, however. The Wisconsin H α Mapper (WHAM) survey [100] will produce a Fabry-Perot map in H α of the northern sky with a 1° resolution. Early results [52] have revealed several very long ($\sim 30^\circ - 80^\circ$) filaments reaching high Galactic latitudes (up to $b \simeq 50^\circ$), superimposed on the diffuse H α background, without a clear correspondence to the other phases of the interstellar medium, observed at 21cm or by radio continuum, far-IR or X-ray surveys. High resolution ($\sim 1'$) imaging surveys of the H α emission in the northern and in the southern emisphere, respectively, are underway by [28] and [46].

The four-year COBE DMR sky maps at different frequencies have been utilized [68] to isolate emission with antenna temperature which varies proportional to frequency to the -2.15 power ($\propto \nu^{-2.15}$) in an attempt to provide a large angular scale map of free-free emission at 53 GHz. This low-signal to noise map is consistent with the H α large scale model with a free-free half height amplitude of $10 \pm 4 \mu$ K. The rms free-free signal on a 7° scale was estimated to be $\Delta T_{\text{ff}} = 7 \pm 2 \mu$ K.

Leitch et al. [74] looking near the NCP found emission with an approximate -2 spectral index. Their analysis indicates a free-free level some 5–10 times that found for the NCP based upon an extrapolation in angular power spectra from [68] or from the H α emission. Moreover their estimates are above those deduced from

the Tenerife experiments. Not surprisingly, the free-free emission is partially correlated with dust as the H α emission has long been known to be. However, there are things that are not understood well and surprises may be lurking (see next section on dust). Planck will clearly have a role in helping to understand the free-free emission.

Dust emission

The dust in our galaxy is heated by the interstellar radiation field (ISRF), absorbing optical and UV photons and emitting the energy in the far IR. The balance between absorption and emission depends on the intensity of the ISRF and the details of the dust, but in general it results in an equilibrium temperature of 18–20 K, in the limit of large dust grains. The emission spectrum from a greybody at this temperature peaks at $\sim 140\mu\text{m}$ but extends out to microwave wavelengths. Adequate removal of dust contamination from the microwave background signal will allow both greater sky coverage and finer spatial resolution.

The new Berkeley-Durham dust map [104] is based on infra-red radiation from the dust, observed by IRAS at $100\mu\text{m}$ and by DIRBE at $100\mu\text{m}$ and $240\mu\text{m}$. The DIRBE $100\mu\text{m}$ map was used to clean up and calibrate the IRAS Sky Survey Atlas (ISSA) and ~ 5000 point sources were removed using positions from the 1.2Jy survey (Fisher et al. 1996). A low-resolution temperature map was derived from the DIRBE $100\mu\text{m}$ and $240\mu\text{m}$ data, which is then applied to the high-resolution map.

Draine & Lazarian [33] have recently proposed that spinning dust grains can produce significant signal peaking in the few 10's of GHz. Another mechanism of dust microwave emission is based on magneto-dipole emissivity [34]. While there is no compelling evidence to support these hypotheses, it is still a lesson to us that there could be surprising new contributions or variation in Galactic emission awaiting us. This indeed is a primary reason that Planck carries a complement of frequencies.

Galactic point sources

Planck measurements will detect the brightest discrete Galactic radio sources, bridging the gap between ground based observations, mostly confined to frequencies $\leq 8\text{GHz}$, and far-IR data, mostly from IRAS and therefore at $\nu \geq 3 \times 10^3\text{GHz}$. As described below for some representative classes of sources, Planck observations will provide crucial information on their physical properties. Also these observations will be unique in investigating the possible existence of extremely compact thermal or non thermal sources, self absorbed up to tens of GHz and therefore unlikely to be found in existing surveys.

Optically thick synchrotron emission gives a strongly inverted spectrum ($S_\nu \propto \nu^{5/2}$), independent of the energy distribution of electrons, producing a low frequency cutoff. For very compact, high density regions, cutoff frequencies as high as several GHz are observed. Likewise, compact and dense HII regions may be optically thick, and have an inverted spectrum ($S_\nu \propto \nu^2$) up to relatively high frequencies.

Supernova remnants (SNR) constitute a particularly bright and well studied class of Galactic radio sources. Nevertheless, existing compilations are believed to be very incomplete, especially with respect to young, bright and older, extended remnants (see [120] for a review).

The broad general category of SNRs actually encompasses a variety of objects with widely different properties, which have been divided into at least 4 subcategories. Their radio emission is non-thermal, with spectral indices α ($S_\nu \propto \nu^{-\alpha}$) generally in the range 0.1–0.9. Planck is expected to detect a large fraction of the 145 SNRs listed by Green (1984); more than half of them will be resolved. Planck will be particularly effective in studying the flat spectrum plerionic SNRs, which are possibly related to type II SN and derive their energy from the rotational energy losses of a central neutron star, rather than being powered by the shock wave of the SN explosion, like the other classes of SNRs. The Planck survey will greatly help in obtaining complete samples of SNRs of the different classes, and in particular will allow to assess the, still debated, abundance of plerionic SNRs and to derive more reliable estimates of their birthrates. Moreover, the Planck mission will provide accurate measurements of the continuum spectrum of the brightest SNRs such as the Crab Nebula and Cassiopeia A, still poorly known in the Planck frequency range. The Planck data will be valuable to investigate the high frequency behaviour of the synchrotron spectrum (and hence the energy distribution of relativistic electrons within these SNRs) and the content of cold dust.

An outstanding mm source is *Sagittarius A*. This source, located at the dynamical center of the Galaxy and presumed to be associated with a supermassive black hole ($M \sim 2.5 \times 10^6 M_\odot$ [36]) has been a puzzle for

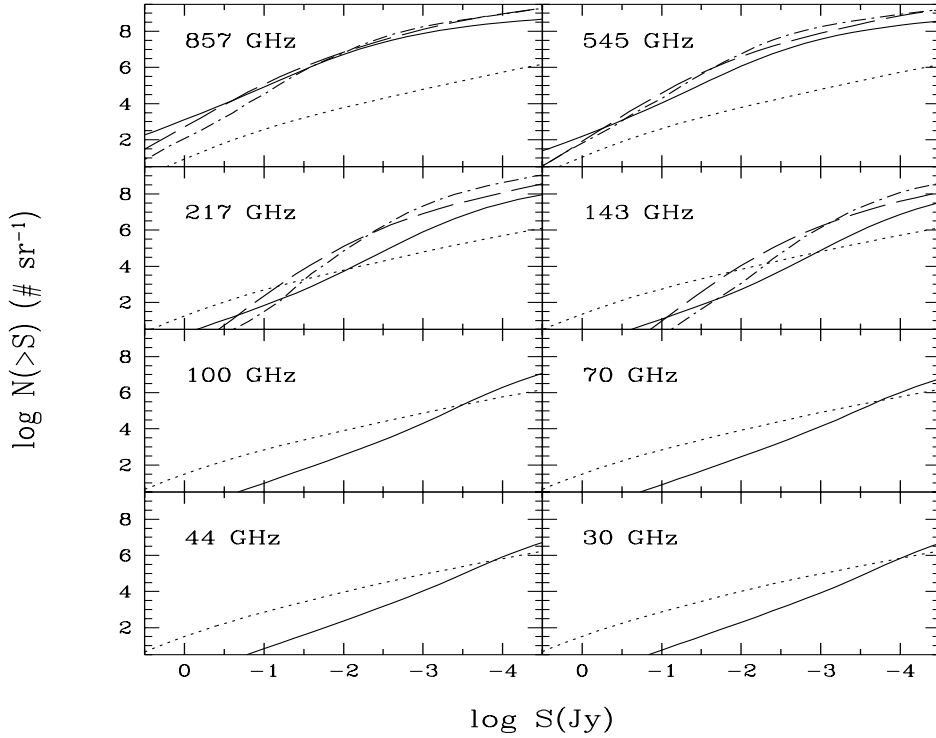


FIGURE 1. Counts of extragalactic sources in Planck channels. The dotted and the solid lines shows the $\log N - \log S$ of radio sources and of dusty galaxies, respectively, predicted by Toffolatti et al. (1998) (see text). The dashed and dot-dashed lines correspond, respectively, to model E of Guiderdoni et al. (1998) and to the kinematic model by Smail et al. (1997); these models take into account only dusty galaxies.

many years (see e.g. [84]). It is brightest in the radio/mm region. Its radio spectrum appears to have an ankle at around $\nu \simeq 84$ GHz, where it steepens from $S_\nu \propto \nu^{0.2}$ to $S_\nu \propto \nu^{0.8}$, and is variable. Planck covers this particularly interesting region and will provide simultaneous measurements at various frequencies.

An extensive survey of millimeter continuum emission from stars was carried out by [3]. A review of the subject has been published by [89]. Massive radiatively driven winds from hot stars have mm radio spectra dominated by optically thick free-free emission with $S_\nu \propto \nu^{2/3}$. The two brightest sources of this class are η Carinae with a variable 1 mm flux of up to 16 Jy [23], making it probably the brightest stellar source at mm wavelengths, and MWC 349 with a flux of 1 Jy at 3 mm. Optically thick free-free emission at mm wavelengths, with fluxes up to 1.5 Jy, is also observed from *symbiotic stars* [106,62], a class of active binaries involving mass transfer from a red giant to a compact, hot companion. The transition to the optically thin regime occurs at about 100 GHz for V1016 Cyg [106] and, in general, should not exceed 1 THz, i.e. is probably in the range covered by the Planck mission. Hot stars with shells, an heterogeneous class of objects, frequently have mm fluxes in the range 100-500 mJy, reaching up to 1.6 Jy. Their radio spectra usually have a turnover from optically thick to optically thin free-free emission around 5–10 GHz. The radio continuum spectra of *planetary nebulae* at GHz frequencies are generally consistent with optically thin free-free emission from the circumstellar material ionized by the hot central remnant. However a few cases are known of strongly inverted spectra, indicating optically thick emission up to 10 GHz (e.g. [66]).

Extragalactic sources

The minimum of the spectral energy distribution for most classes of sources occurs at a few mm wavelengths, i.e. close to the peak frequency of the CMB. This is due to the steep increase with frequency of the dust emission spectrum in the mm/sub-mm region (typically $S_\nu \propto \nu^{3.5}$), which makes the crossover between radio and dust

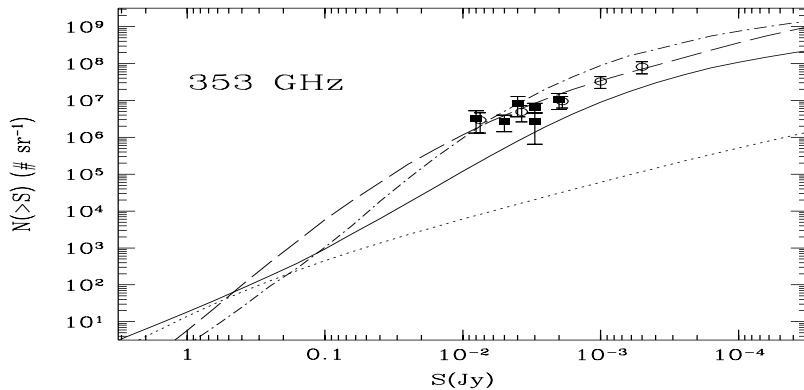


FIGURE 2. A comparison of predictions by the same models as in Fig. 1 with the 850 μm galaxy counts obtained by different groups (for references see Smail et al. 1998) with the Sub-millimeter Common User Bolometer Array (SCUBA) on the 15-m James Clerk Maxwell Telescope (JCMT) at Mauna Kea.

emission components only weakly dependent on their relative intensities; moreover, dust temperatures tend to be higher for distant high luminosity sources, partially compensating for the effect of redshift.

A consequence is that there is an abrupt change in the source populations of bright sources observed in channels above and below $\sim 1\text{ mm}$: radio sources dominate at longer wavelengths, while in the sub-mm region the Planck instruments will mostly see dusty galaxies (see Figs. 1 and 2).

By simply looking for peaks more than 5σ above the mean, we can recover sources brighter than a few to several hundred mJy, the exact value depending on the angular resolution of each channel and on the model dependent confusion noise (see e.g., [115]). It may be noted that only a negligible fraction ($\simeq 3 \times 10^{-7}$ in the case of gaussian fluctuations) of true CMB anisotropies are misinterpreted as discrete sources by this approach.

Methods have been devised, allowing us to recover point sources from Planck maps to substantially fainter flux levels. Tegmark & de Oliveira Costa [113] derived an optimal filter in the Fourier domain, exploiting the point-like nature of sources, as opposed to the diffuse CMB and Galactic emissions, to suppress the latter components. They showed that this method improves the ability to detect sources by factors between 2.5 and 18, depending on the channel.

Hobson et al. [59] applied a maximum entropy method to analyse simulated Planck observations. By introducing information about the power spectrum of point sources in each frequency channel and the correlations between frequencies, they were able to effectively recover point sources down to 60 mJy for the 44 and 353 GHz channels, chosen because they lie near the centres of the frequency ranges of the LFI and HFI, respectively.

Ground based instruments, such as SCUBA on JCMT or the large mm/sub-mm arrays planned for the next decade, or dedicated space missions, such as FIRST, will go much deeper but over small areas. For example, the SCUBA's field of view is $\sim 6\text{ arcmin}^2$, and the surveys carried out so far have covered areas between 0.002 and 0.1 square degrees, so that counts could be estimated only for sources fainter than about 10 mJy (see Fig. 2). The field of view of the Large Millimeter Array is expected to be $\sim 50''$; about one month of observing time would be required to survey 2 square degrees to a sensitivity of 0.9 mJy (5σ ; see [101]). The SPIRE photometer on FIRST, which has three bands with nominal wavelengths of 250, 350, and 500 μm , has a $4'$ field of view; a survey of 4 square degrees to a 5σ limit of 6.5 mJy would take about 1000 hours of observations [49].

On the other hand, the full sky coverage of the Planck surveys makes it possible to determine the source counts up to Jy levels, i.e. to extend them by about two orders of magnitude in flux. A broad range in fluxes is obviously essential to study the epoch dependent luminosity function.

A further important foreground component of the microwave sky is produced by the Sunyaev-Zeldovich effect in clusters of galaxies, whose flux changes of sign at mm wavelengths, passing through 0 at 217 GHz.

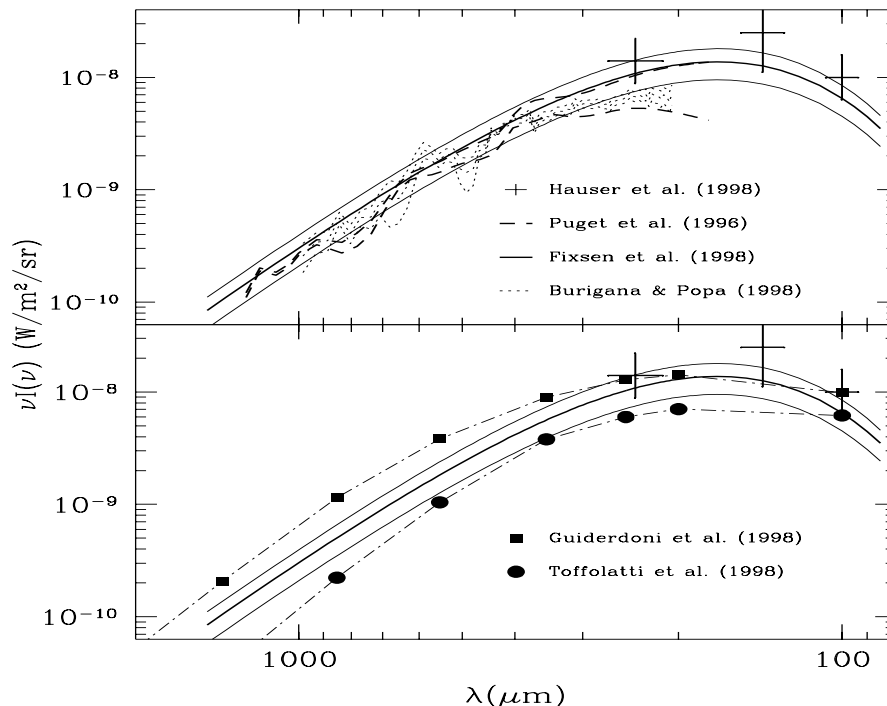


FIGURE 3. Recent determinations of the spectrum of the extragalactic far-IR to mm background compared with model predictions.

Physics of Active Galactic Nuclei

Planck covers the frequency range where the shape of the spectral energy distribution of Active Galactic Nuclei is least known and where important spectral features, carrying essential information on physical conditions of sources, show up.

Observations at mm/sub-mm wavelengths often reveal the transition from optically thick to optically thin radio emission in the most compact regions. The self absorption frequency carries information on physical parameters. A systematic survey in the 30–900 GHz range will, for example, allow us to see if there are systematic differences in the synchrotron turnover frequencies between e.g. BL Lacs and quasars, as would be expected if BL Lac emission is angled closer to our line of sight so that their turnovers are boosted to higher frequencies. Correlations between turnover frequency and luminosity, which is also boosted by relativistic beaming effects, would help confirm current models.

Major high radio frequency flares have been observed in several compact radio sources (e.g. PKS 0528+134, 3C 345, ...). There are indications that the peak emission moves to lower frequencies as it ages. Planck may catch the rise of the flare at the highest frequencies, missed by ground based observations.

Establishing the peak of the synchrotron emission is crucial also to understand if the emission at higher energies is to be attributed to Compton scattering of the same synchrotron photons (synchrotron self-Compton) or of seed photons external to the synchrotron emitting region.

The spectral break frequency, ν_b , at which the synchrotron spectrum steepens due to electron energy losses, is related to the magnetic field and to the “synchrotron age” t_s (in Myr) by: $\nu_b \simeq 96(30 \mu\text{G}/B)^3 t_s^{-2}$ GHz. The systematic multifrequency study at the Planck frequencies will thus provide a statistical estimate of the radiosource ages.

Excess far-IR/sub-mm emission, possibly due to dust, is often observed from radio galaxies [67]. Planck data will allow us to assess whether this is a general property of these sources; this would have interesting implications for the presence of interstellar matter in the host galaxies, generally identified with giant ellipticals, which are usually thought to be devoid of interstellar matter.

Flat-spectrum radio sources

To date, the most detailed predictions of radio source counts at Planck frequencies are those worked out by [115]. The dotted line in Figs. 1 and 2 shows the predictions of a variant of their model, whereby the spectra of “flat”-spectrum sources keep an $\alpha = 0$ slope up to frequencies of 1 THz, steepening to $S_\nu \propto \nu^{-0.75}$ at higher frequencies.

Sokasian et al. [111] have produced skymaps of bright radio sources at frequencies up to 300 GHz by means of detailed individual fits of the spectra of a large number of sources compiled from a number of catalogs, including the all sky sample of sources with $S_{5\text{ GHz}} \geq 1\text{ Jy}$ (Kühr et al. 1991). Their estimated number of sources brighter than $S_{90\text{ GHz}} = 0.4\text{ Jy}$ is about a factor of two below that predicted by [115]. A very similar result was obtained by [61] based on the observed distribution of 8.4–90 GHz spectral indices. On the other hand, these empirical estimates yield, strictly speaking, lower limits, since sources with inverted spectra may be under-represented in the primary sample. Furthermore, in the presence of substantial variability, estimates using mean fluxes underestimate actual counts of bright sources [31]. Anyway, as mentioned by [111], it is very encouraging that so different approaches yield results close to each other.

As shown by Fig. 1, the models by [115] predict that, at least for fluxes brighter than 0.1 Jy, counts are dominated by radio sources for frequencies up to 217 GHz. These sources are therefore expected to have a considerable impact on CMB anisotropy measurements.

Radio sources with strongly inverted spectra

As already mentioned, classes of sources are known with strongly inverted spectra, peaking at high frequencies, that would be either missing from, or strongly under-represented in low frequency surveys.

GHz Peaked Spectrum radio sources (GPS) appear to have a fairly flat distribution of peak frequencies extending out to 15 GHz in the rest frame [88], suggesting the existence of an hitherto unknown population of sources peaking at mm wavelengths [24,71]. De Zotti et al. [30] suggested that from several tens to hundreds of GPS sources could be detected by Planck. Thus, although these rare sources will not be a threat for studies of CMB anisotropies, we may expect that the Planck surveys will provide crucial information about their properties. GPS sources are important because they may be the younger stages of radio source evolution [43,95] and may thus provide insight into the genesis of radio sources; alternatively, they may be sources which are kept very compact by unusual conditions (high density and/or turbulence) in the interstellar medium of the host galaxy [116].

High frequency free-free self absorption cutoffs may be present in AGN spectra. Ionized gas in the nuclear region free-free absorbs radio photons up to a frequency:

$$\nu_{\text{ff}} \simeq 50 \frac{g}{5} \frac{n_e}{10^5 \text{ cm}^{-3}} \left(\frac{T}{10^4 \text{ K}} \right)^{-3/4} l_{\text{pc}}^{1/2} \text{ GHz} . \quad (2)$$

Free-free absorption cutoffs at frequencies $> 10\text{ GHz}$ may indeed be expected, in the framework of the standard torus scenario for type 1 and type 2 AGNs, for radio cores seen edge on, and may have been observed in some cases [11]. They provide constraints on physical conditions in the parsec scale accretion disk or infall region for the nearest AGNs.

Planck may also allow us to study the nearest examples of another very interesting class of radio sources, powered by advection-dominated accretion flows [85,42,32]. These may correspond to the final stages of accretion in large elliptical galaxies hosting a massive black hole. Their radio emission is characterized by an inverted spectrum with $S_\nu \propto \nu^{0.4}$ up to frequencies of 100–200 GHz, followed by fast convergence.

Evolving dusty galaxies

Shown in Figs. 1 and 2 are the counts predicted by the models of [115], [50] (model E) and [109]. The former model falls somewhat short of the recent SCUBA counts at $850\text{ }\mu\text{m}$ (Fig. 2) as well as of the far-IR to mm extragalactic background intensity (Fig. 3) determined by [55,44]. On the other hand, the model by [50] overpredicts the background intensity at $\lambda > 350\text{ }\mu\text{m}$. The model by [109] yields a background intensity far in excess of the observational limits and will not be considered further.

The Sunyaev-Zeldovich effect

Another important astrophysical foreground for CMB observations are clusters of galaxies. As predicted by [112] the inverse Compton scattering of CMB photons against the hot and diffuse electron gas trapped in the potential well of cluster of galaxies, and responsible for their X-ray emission, yields a systematic shift of photons from the Rayleigh-Jeans to the Wien side of the spectrum. This “thermal” effect, arising from the thermal motions of the electrons, is described by the Kompaneets [69] equation which, in the non relativistic limit [for a discussion of the relativistic Sunyaev & Zel’dovich (hereafter SZ) effect see, in this volume, Itoh, Rephaeli and Sunyaev], leads to the familiar expression for the (spectral) intensity change across a cluster:

$$\Delta I_\nu = 2 \frac{(kT_{CMB})^3}{(hc)^2} yg(x) \quad (3)$$

where T_{CMB} is the CMB temperature and $x = h\nu/kT_{CMB}$. The spectral form of this “thermal effect” is described by the function $g(x) = x^4 e^x [x \cdot \coth(x/2) - 4]/(e^x - 1)^2$, which is negative (positive) at values of x smaller (larger) than $x_0 = 3.83$, corresponding to a critical frequency $\nu_0 = 217$ GHz. The Comptonization parameter is

$$y = \int \frac{kT}{mc^2} n_e \sigma_T dl, \quad (4)$$

where n_e and T are the electron density and temperature, σ_T is the Thomson cross section, and the integral is over a line of sight through the cluster.

The main emphasis so far has been on the measurement of the SZ effect in individual clusters [see [13] for a review and Birkinshaw (this volume)]. On the other hand, because of its angular resolution and sensitivity, Planck is expected to observe a substantial number of clusters. In fact, with respect to the incident radiation field, the change of the CMB intensity across a cluster can be viewed as a net flux emanating from the cluster, negative below the crossover frequency ν_0 and positive above it:

$$\overline{\Delta F}_\nu(\hat{\gamma}_\ell) = 2 \frac{(kT_{CMB})^3}{(hc)^2} y_o(\hat{\gamma}_\ell; M, z) \Xi(\hat{\gamma}_\ell; M, z) \left[\int dx g(x) E(x) / \int dx E(x) \right] \quad (5)$$

In the previous expression M is the cluster mass, $\hat{\gamma}_\ell$ is the line of sight passing through the cluster center, y_o is the Comptonization parameter along it, $E(x)$ is the frequency response of the receivers and the geometrical factor Ξ is given by

$$\Xi(M, z) = \int d\Omega R_s(|\hat{\gamma}_l - \hat{\gamma}|) \zeta(\hat{\gamma}, M, z) \quad (6)$$

where ζ is the intra-cluster (IC) gas profile and R_s is the angular response of the antenna.

Thus, the predicted number counts for SZ clusters are simply:

$$N(> \overline{\Delta F}_\nu) = \int \frac{dV}{dz} dz \int_{\overline{M}(\overline{\Delta F}_\nu, z)} dM N(M, z) \quad (7)$$

where $N(M, z)$ is the cluster mass function and the lower bound of the mass integral is determined by requiring that clusters of mass $M > \overline{M}$ at redshift z have SZ fluxes (averaged over the receiver pass-band and measured by an antenna of given angular resolution) greater than $\overline{\Delta F}_\nu$ (for details see, e.g., [21]).

Theoretical calculations of SZ cluster counts have been performed using a Press & Schechter [92] formalism by [25, 10, 37, 21]. In Fig. 4 we show a comparison of the published SZ counts for a flat cosmological model with Hubble constant of $H_0 = 50 \text{ km s}^{-1} \text{ Mpc}^{-1}$. The differences in the SZ number counts are due to different assumptions and to the large uncertainties that we still have in the theoretical modelling of the effect. In short, the differences are due to the following points:

- *density fluctuation power spectrum*: [25] and [10] use a simple power law power spectrum [$P(k) = Ak^n$] with spectral index of $n = -1$ and $n = -1.85$, respectively; [37] and [21] use scale-invariant initial conditions and take into account the transfer function appropriate for Cold Dark Matter-like models [$P(k) = AkT_{CDM}^2(k)$].

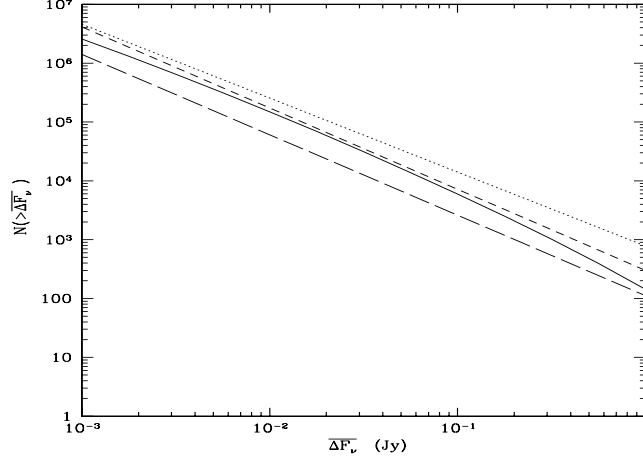


FIGURE 4. Comparison between the number counts in a flat universe calculated according to Barbosa et al. (dotted line), De Luca et al. (dashed line), Eke et al. (long-dashed line), Colafrancesco et al. (continuous line). These counts refer to the frequency of 400 GHz, except for those by Eke et al., which refer to 545 GHz. Note that a SZ source is only roughly half as intense at 545 GHz as it is at 400 GHz; this partially explains why the Eke et al. curve is low.

- *Normalization of the density fluctuation power spectrum:* The amplitude of the power spectrum is normalized a posteriori in order to fit cluster observations; [25] normalize this amplitude in order to recover the cluster mass function of Bahcall & Cen [7], while [10] normalize it to the cluster temperature function of [57]; [21] normalize A to the X-ray luminosity function of [70] (see also [20]), while [37] derive the integrated cluster temperature function from the original [57] catalogue and use this function to normalize A .
- *Mass-Temperature relation:* simple scaling laws are used to derive, under the hydrostatic equilibrium hypothesis, the relation between the mass and the temperature of a cluster (see, e.g., [10]):

$$T(M, z) = T_{15} \Omega_0^{1/3} h^{2/3} \left[\frac{\Delta_c(\Omega_0, z)}{180} \right]^{1/2} \left(\frac{M}{M_{15}} \right)^{2/3} (1+z) \quad (8)$$

Here Δ_c is the non-linear density contrast of a cluster that collapsed at redshift z , while T_{15} is the temperature of a cluster of $M_{15} = 10^{15} h^{-1} M_\odot$ which collapses today. De Luca et al. and Barbosa et al. [25,10] renormalize T_{15} to 6.8 keV, a value suggested by the numerical simulation of [39]; Colafrancesco et al. [21] normalize to 5.8 keV, while [37] use for T_{15} the value of 7.5 keV, which is in good agreement with their N-body simulations. Normalizing the amplitude of $P(k)$ to the cluster temperature function minimizes the effect of different choices of T_{15} .

- *intra-cluster mass fraction:* the IC gas mass, M_g , is often assumed to be a fixed fraction of the total cluster mass: $f_g \equiv M_g/M$. De Luca et al. and Barbosa et al. [25,10] made their calculations assuming a constant IC gas mass fraction $f_g = 0.2$, while Eke et al. and Colafrancesco et al. [37,21] use $f_g = 0.1$.

The modelling of the IC gas is a critical issue to be discussed. According to a numbers of theoretical models (see e.g. [64,40,19]) f_g is not just a constant and can be written as follows:

$$f(M, z) = f_0 \left(\frac{M}{M_{15}} \right)^\eta (1+z)^\xi. \quad (9)$$

where f_0 is a constant and η is assumed to be independent of M : this is a good approximation if one considers only massive clusters (see [18]). This simple parameterization (originally proposed by [17]) together with simple scaling laws provides in the case of a flat universe (see, e.g., [81]):

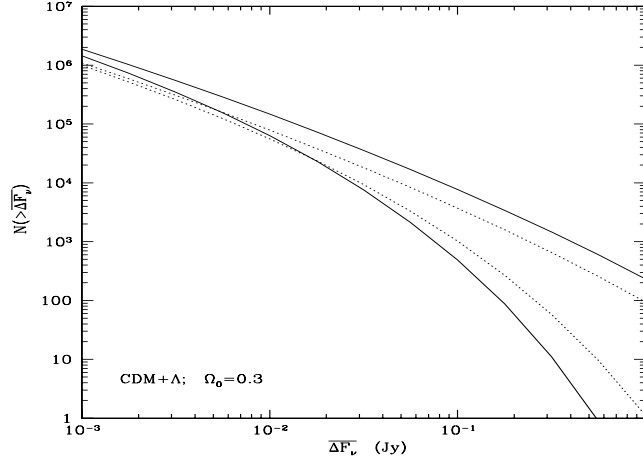


FIGURE 5. SZ cluster number counts for a low density, vacuum-dominated CDM model with $\Omega_0 = 0.3$. The heavy lines represent the expected counts for the Planck/HFI 353 GHz (continuous line) and Planck/LFI 100 GHz (dotted line) channels. The light lines are the expected counts without taking into account the receiver angular resolution.

$$L \propto T^{2+3\eta}(1+z)^{3(1-2\eta-2\xi)/2}. \quad (10)$$

From the observational point of view, the luminosity/temperature relation, $L \propto T^\alpha$, for X-ray clusters has been derived by several authors. As initially discussed by [41], the intrinsic dispersion of these $L - T$ relation is drastically reduced when corrections are made for the existence of cooling flows, thus providing a determination of the slope $\alpha \sim 2.6$, with a precision $\gtrsim 5\%$ [1,80,4]. Using the cluster catalogues of [1] and [80], Reichart et al. [97] derived the values $\eta = 0.22^{+0.08}_{-0.07}$ and $\xi = 0.35^{+0.35}_{-0.33}$. This ξ value, appropriate for a flat universe, lowers to $\xi = 0.14^{+0.35}_{-0.33}$ for $\Omega_0 \rightarrow 0$. Thus, cluster formation is not a self-similar process: the mass of the IC gas is not a fixed fraction of the cluster total mass. The values of ξ derived by [97] provide very little evolution of the $L - T$ relation up to redshift $\lesssim 0.5$, as found by [83] with the ASCA data.

Eke et al. [38] showed that the cluster temperature function, both locally and at $z \sim 0.3$ [58], is best fitted by a low-density, vacuum dominated, CDM model with $\Omega_0 = 0.3$. According to these authors, a flat universe is ruled out at the 98% confidence level [58,38] (see, however, [103], who find $\Omega_0 = 0.85 \pm 0.2$). In Fig. 5 we show the SZ number counts expected for a CDM+ Λ model ($\Omega_0 = 0.3$) with the angular resolution of the Planck/HFI 353 GHz and Planck/LFI 100 GHz channels, respectively. Resolution matters, because the flux collected by an antenna of angular resolution σ_B , pointing at the cluster center, is only a fraction of the total one for those clusters whose extension is larger than σ_B . This effect, taken into account by [21], tends to suppress cluster counts at high fluxes, as one loses the less massive and more local clusters. These clusters may be recovered by a suitable smoothing of the original map, which will bring out large, coherent regions with a higher signal to noise ratio. This effect is shown in Fig. 5 where we use $\eta = 0.2$ and $\xi = 0.3$: lowering ξ to 0.15 (the value found by [97] for $\Omega_0 = 0$) increases the SZ number counts by only 10%.

The number of clusters that Planck will be able to observe critically depends on the efficiency in separating Planck observations into different physical components (for a discussion on this point see [60] and references therein). In any case it should be possible to select and measure a number of clusters, even without any component separation. The Planck detection of SZ clusters may provide an independent estimate of Ω_0 (see, e.g., [10]; see however [118] for a different point of view), complementing the more precise one arising from the measurement of the angular power spectrum of the primary CMB anisotropy. The comparison of SZ and X-ray measurements will yield an independent measure of the Hubble constant [16] (see [13] for a recent review). If the temperature structure of the cluster is simple, the relation between the SZ flux and the X-ray temperature of a cluster provides a measure of the IC gas mass, independently of how the IC gas is distributed. This is due to the linear dependence of the SZ effect on the electron density. Finally, the correlation between the SZ signal and the X-ray luminosity will provide an interesting, complementary tool for studying the dependence of the IC gas properties on the cluster mass and the cosmological epoch [22].

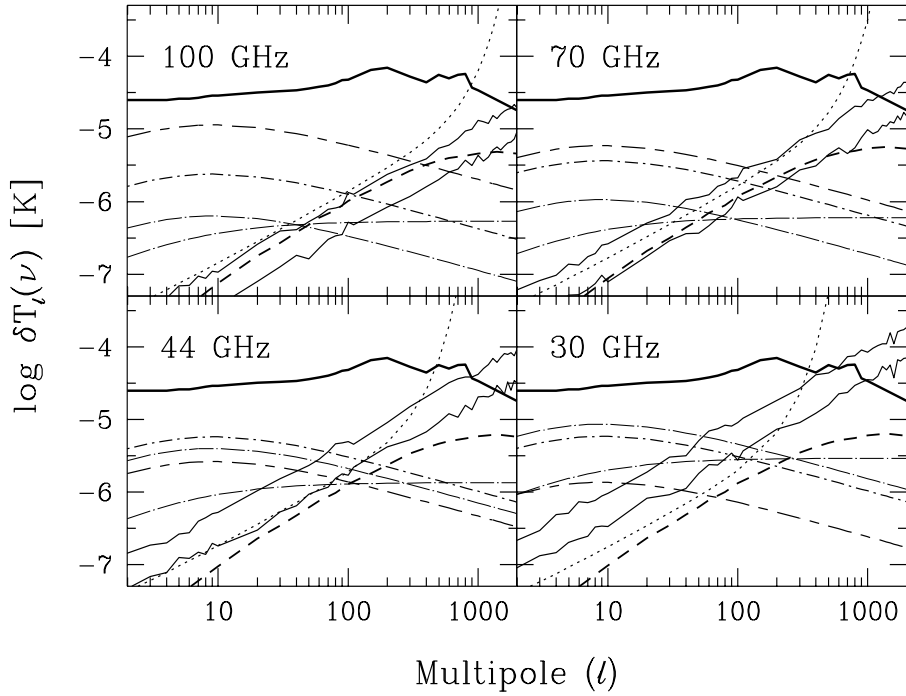


FIGURE 6. Angular power spectra of the components contributing to fluctuations at the LFI frequencies. Following Tegmark & Efstathiou (1996), we have plotted, for each component, the quantity $\delta T_\ell(\nu) = [\ell(2\ell + 1)C_\ell(\nu)/4\pi]^{1/2}$. The upper heavy solid curve shows the power spectrum of CMB fluctuations predicted by the standard CDM model ($\Omega = 1$, $H_0 = 50 \text{ km s}^{-1} \text{ Mpc}^{-1}$, $\Omega_b = 0.05$). Fluctuations in the Galactic emissions at $|b| > 30^\circ$ are represented by long+short dashes (dust), dots+short dashes (free-free), and dots+long dashes (synchrotron). For the power spectrum of the synchrotron emission we have plotted both the power spectrum derived by Tegmark & Efstathiou (1996) and that observed in the Tenerife patch (Lasenby 1996); the latter is significantly lower than the former in the range of scales where it has actually been measured, but has a flatter slope so that it may become relatively more important on small scales; it may be noted however, that the power spectrum must fall off on scales smaller than the coherence length of the emitting blobs. The roughly diagonal solid lines show the contributions of extragalactic sources, neglecting the effect of clustering and assuming that sources brighter than 1 Jy (upper line) or 0.1 Jy can be identified and removed. The heavy dashed line peaking at large ℓ shows the power spectrum of anisotropies due to the Sunyaev-Zeldovich effect computed by Atrio-Barandela & Mücke (1998) adopting a lower limit of $10^{14} M_\odot$ for cluster masses, a present ratio $r_{\text{virial}}/r_{\text{core}} = 10$, and $\epsilon = 0$. The dotted line shows the unsmoothed noise contribution of the instrument.

POWER SPECTRA OF FOREGROUND FLUCTUATIONS

The angular power spectrum of the Galactic synchrotron emission can be determined from large scale radio maps, particularly from those at 408 and 1420, after removing the baseline stripes which contain power on angular scales of a few to ten degrees [26]. Lasenby [71] has used the 408 and 1420 MHz surveys to estimate the spatial power spectrum of the high latitude region surveyed in the Tenerife experiments and found an angular power spectrum slightly flatter than ℓ^{-2} for $\ell \leq 300$. A steeper mean power spectrum ($\propto \ell^{-3}$), i.e. with the same dependence on ℓ as the dust and free-free emissions, was estimated by [114].

Kogut et al. [68] have compared the COBE DMR maps with the DIRBE maps and found a correlation between the free-free and dust emission. On 7° angular scales they concluded that the spatial power law index is -3.0 , a well-determined value for dust and HI on degree scales. This was confirmed to some extent by [29] for the north celestial polar cap in a correlation of Saskatoon data with the IRAS & DIRBE maps.

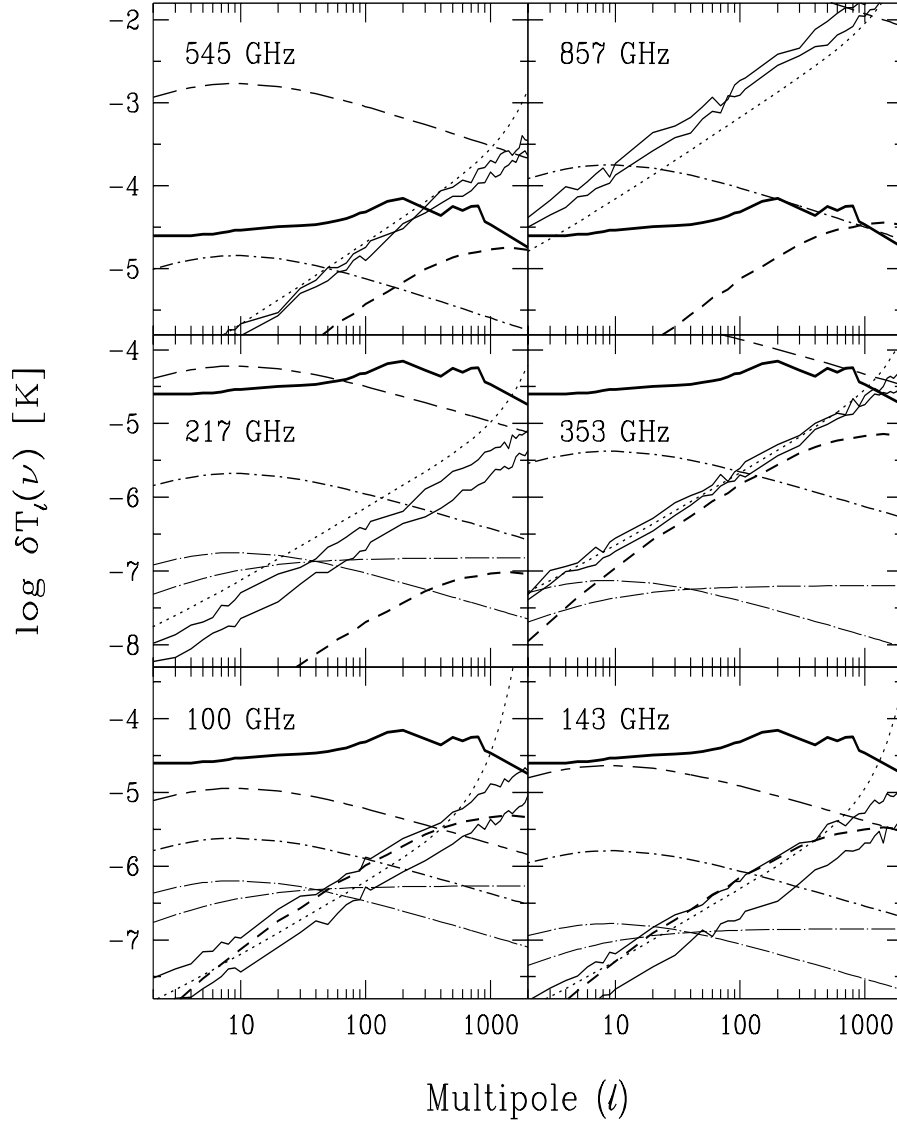


FIGURE 7. Same as in Fig. 6, but for HFI frequencies. The lines have the same meaning as in Fig. 6. Note that the Sunyaev-Zeldovich effect vanishes at 217 GHz. However, integrating over the bandwidth of the Planck/HFI channel centered at that frequency, a small but non vanishing signal is found.

The $H\alpha$ images of the North Celestial Pole (NCP) area made by [45] have been analyzed by [117] to provide an estimate of the spatial power spectrum on scales of $10'$ to a few degrees. The slope they find, $C_{\text{ff}} \propto \ell^{-2.27 \pm 0.07}$, is significantly flatter than that inferred by [68] from COBE data; however the rms amplitude is considerably lower, $\simeq 0.25 \text{ cosec}(|b|) \mu\text{K}$ on $10'$ scales at 53 GHz assuming a gas temperature $\sim 10^4$ K, resulting in a lower signal at all scales of interest.

The global power spectrum of dust emission fluctuations was determined by [47], based on IRAS $100 \mu\text{m}$ data, to be $C_{\text{dust}} \propto \ell^{-3}$ in the 8° – $4'$ range. Wright [122], from an analysis of COBE/DIRBE data with two methods, also found, at high galactic latitude, $C_{\text{dust}} \propto \ell^{-3}$ for $2 < \ell < 300$. The Schlegel et al. [104] analysis of their combined DIRBE and IRAS dust maps suggests a shallower slope, $C_{\text{dust}} \propto \ell^{-2.5}$, with variations from place to place.

For $\ell < 300$, corresponding to angular scales $> 30'$ [$\ell \simeq 180^\circ/\theta(\text{deg})$], diffuse Galactic emissions dominate

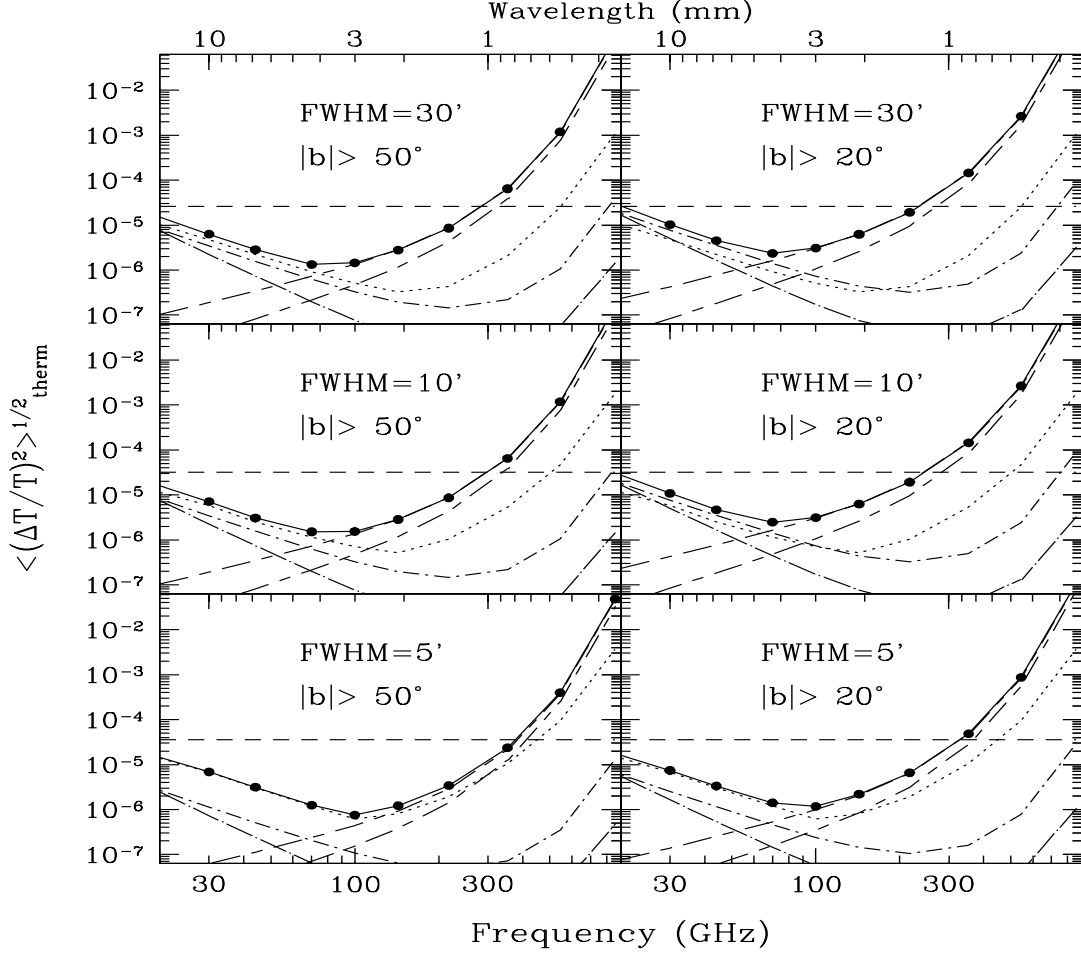


FIGURE 8. Temperature fluctuations as a function of frequency for three angular scales and two cuts in galactic latitude. The horizontal dashed line shows the expected level of primordial CMB anisotropies according to the standard CDM model. The average contributions from Galactic free-free, synchrotron and dust emissions are represented by dots+short dashes, dots+long dashes, and long+short dashes, respectively. The lower long/short dashed curve shows a lower limit to Galactic dust emission fluctuations. The dotted curve gives the fluctuation level yielded by discrete extragalactic sources fainter than 100 mJy, computed after the Toffolatti et al. (1998) model (see text). The solid line is the quadratic sum of contributions from all foreground components; the filled circles on it mark the Planck frequencies.

foreground fluctuations even at high Galactic latitudes. These are minimum at $\nu \simeq 70$ GHz [68]. For larger values of ℓ the dominant contribution is from extragalactic sources; their minimum contribution to the anisotropy signal occurs around 150-200 GHz.

A Poisson distribution of extragalactic point sources produces a simple white-noise power spectrum, with the same power in all multipoles. Correspondingly, the point source fluctuations become increasingly important with decreasing angular scale (i.e., with increasing ℓ). Thus the minimum in the global power spectrum of foreground fluctuations moves, at high galactic latitudes, from about 70 GHz for $\ell < 300$, where Galactic emissions dominate, to 150-200 GHz at higher values of ℓ (the exact value of the frequency of the minimum depends on the detailed spectral and evolutionary behaviour of sources). For the same reason, the frequency of minimum foreground fluctuations decreases with decreasing Galactic latitude.

Figures 6 and 7 show the expected power spectra of the main foregrounds components in the LFI and HFI channels respectively. It is clear from Fig. 7 that the source removal is much more effective in reducing the fluctuation level at the lowest than at the highest frequencies. This is due to the fact that at $\lambda \gtrsim 1$ mm, fluctuations are dominated by the brightest sources below the detection limit, while at shorter wavelengths the dominant population are evolving dusty galaxies whose counts are so steep (see Fig. 1) that a major

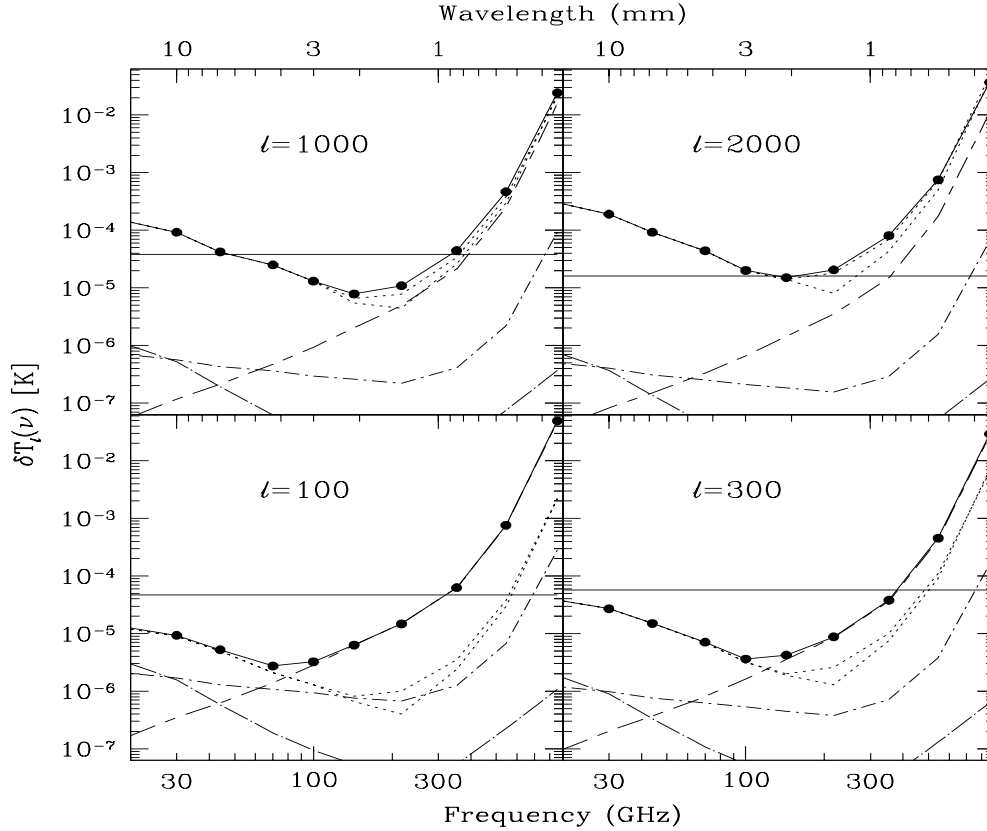


FIGURE 9. Frequency dependence of CMB brightness fluctuations $\delta T_\ell(\nu) = [\ell(2\ell + 1)C_\ell(\nu)/4\pi]^{1/2}$ for different multipoles. The dots+long dashes, dots+short dashes, and long+short dashes correspond to the mean contributions from Galactic foregrounds (synchrotron, free-free and interstellar dust, respectively), at $|b| > 50^\circ$. The dotted lines show the contribution of extragalactic sources (assuming that those brighter than 1 Jy are removed): the lower one corresponds to the Toffolatti et al. (1998) model mentioned in the text; the upper one was obtained summing in quadrature the results of model E by Guiderdoni et al. (1998) for evolving dusty galaxies with the results by Toffolatti et al. (1998) for radio sources. The heavy solid curve is the quadratic sum of all foreground contributions; the filled circles on it identify Planck frequencies. The horizontal line shows the fluctuation level predicted by the standard CDM model.

contribution to fluctuations comes from much fainter fluxes.

Figure 8 illustrates the frequency dependence of rms fluctuations in a beam of FWHM θ for several values of θ , while Fig. 9 shows the frequency dependence of the power spectrum for four values of ℓ .

The effect of clustering

Toffolatti et al. [115] found that clustering contributions to fluctuations due to extragalactic sources is generally small in comparison with the Poisson contribution. However, the latter contribution, at least in the case of radio sources, comes mostly from the brightest sources below the detection limit, while the clustering term is dominated by fainter sources. Therefore, an efficient subtraction of sources decreases the Poisson term much more effectively than the clustering term, which therefore becomes relatively more and more important.

In the case of a power law angular correlation function ($w(\theta) \propto \theta^{1-\gamma}$), the power spectrum of intensity fluctuations is (eq. (58.13) of [90]):

$$C_\ell \propto \ell^{\gamma-3} . \quad (11)$$

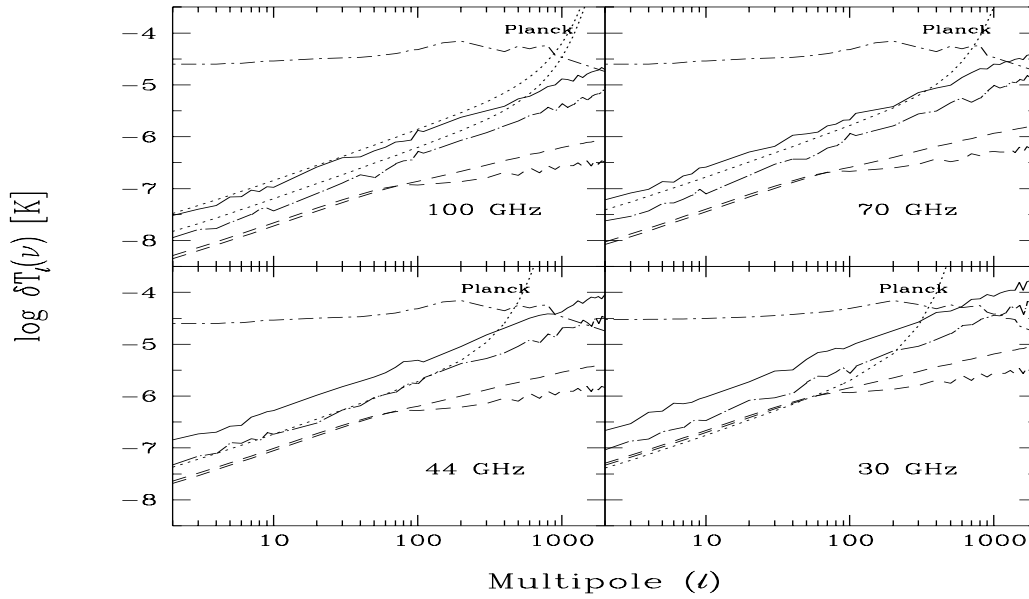


FIGURE 10. Comparison of the Poisson component of the power spectra of radio sources with the component due to clustering. The upper dot/dashed curve shows the primordial CMB power spectrum according to the standard CDM model. The roughly diagonal solid and dot/dashed lines represent the Poisson component for flux cuts of 1 Jy and 0.1 Jy, respectively. The dashed lines show the component due to clustering estimated using the angular correlation functions derived by Loan et al. (1997; lower line) and by Magliocchetti et al. (1998). The dotted lines show the instrumental unsmoothed noise contributions; at 100 GHz there are two lines referring to the LFI (lower) and to the HFI. Only the LFI operates at the other frequencies.

If this behaviour extends to large enough angular scales, i.e. to small enough values of ℓ , the clustering signal will ultimately become larger than the Poisson anisotropy. On the other hand, for large values of θ , $w(\theta)$ is expected to drop below the above power law approximation, and C_ℓ will correspondingly break down.

The preliminary estimates (Toffolatti et al., in preparation) reported in Fig. 10 are based on the correlation functions of radio sources derived by [76] and by [78]. The different slopes at large values of ℓ reflect different values of γ : the upper curve correspond to the larger value ($\gamma = 2.5$) obtained by [78].

Scott & White [105] have recently shown that if dusty galaxies cluster like the $z \sim 3$ Lyman break galaxies, at frequencies ≥ 217 GHz the anisotropies due to clustering may exceed the Poisson ones on all scales accessible to Planck; in the 353 GHz (850 μm) channel the clustering signal may exceed the primordial CMB anisotropies on scales smaller than about 30'. It should be noted, however, that current models [115,50] strongly suggest a broad redshift distribution of sources contributing to the autocorrelation function of the intensity fluctuations, implying a strong dilution of the clustering signal. A further substantial overestimate of the effect of clustering may follow from the extrapolation to degree scales, with constant slope, of the angular correlation function determined on scales of up to a few arcmin. Indeed, a clustering signal much lower than estimated by [105] was found by [115] who modelled the full evolutionary history of galaxies.

POLARIZATION

The polarized foreground spectra have not been studied as extensively as the intensity spectra. For a power law electron energy spectrum $dN/dE = N_0 E^{-p}$, the polarization level, Π , yielded by a uniform magnetic field is [75,48]:

$$\Pi = \frac{3(p+1)}{3p+7} . \quad (12)$$

For a typical high frequency value of $p \sim 3$, $\Pi \sim 75\%$. Non-uniformities of the magnetic fields and differential Faraday rotation decrease the polarization level. However, the Faraday rotation optical depth is proportional to ν^{-2} so that Faraday depolarization is negligible at the high frequencies relevant for Planck.

Free-free emission is not polarized. However, Thompson scattering by electrons in the HII regions where it is produced, may polarize it tangentially to the edges of the electron cloud [65]. The polarization level is expected to be small, with an upper limit of approximately 10% for an optically thick cloud.

The intrinsic polarization of *Galactic dust emission* is estimated to be $\sim 30\%$ [56]. The observed polarization degree is smaller by a factor $\Phi = RF \cos^2 \gamma$ [73], where R and F are the reduction factors due to misalignments of grain axes with the magnetic field and to the different orientations of polarization vectors of different components along any line of sight, while the $\cos^2 \gamma$ accounts for the projection of the direction of polarization on the plane of the sky. The level of polarized emission from Galactic dust at high Galactic latitudes has been estimated by [94]. To ease the comparison with the CMB polarization, they considered two linear combinations of the Stoke's parameters in Fourier space: the E-mode, dominated by scalar perturbations, and the B-mode, produced by tensor perturbations. For Galactic dust polarized emission, the power spectra of the two modes can be approximated by [94]:

$$C_E(\ell) = 8.9 \times 10^{-4} \ell^{-1.3} (\mu\text{K})^2 \quad (13)$$

$$C_B(\ell) = 1. \times 10^{-3} \ell^{-1.4} (\mu\text{K})^2 \quad (14)$$

They concluded that, at frequencies around 100 GHz, the power spectrum of this polarized component is below that of the scalar induced CMB polarization at $\ell \gtrsim 200$, but is above the tensor induced CMB polarization expected for a flat, tilted cold dark matter model with spectral index of scalar perturbations $n_s = 0.9$.

Bouchet et al. [14] have analyzed the possibility of extracting the power spectrum of CMB polarization fluctuations in the presence of polarized Galactic foregrounds using a multifrequency Wiener filtering of the data. They concluded that the power spectrum of E-mode polarization of the CMB can be extracted from Planck data with fractional errors $\lesssim 10\text{--}30\%$ for $50 \lesssim \ell \lesssim 1000$. The B-mode CMB polarization, whose detection would unambiguously establish the presence of tensor perturbations (primordial gravitational waves), can be detected by Planck with signal-to-noise $\simeq 2\text{--}4$ for $20 \leq \ell \leq 100$ by averaging over a 20% logarithmic range in multipoles.

Polarization of *extragalactic sources*, not considered by [14], can be an important issue as well. Flat spectrum radio sources are typically 4-7% polarized at cm and mm wavelengths [86,2]. For random orientations of the magnetic fields of sources along the field of view, the rms polarization fluctuations are approximately equal to intensity fluctuations times the mean polarization degree (De Zotti et al., in preparation).

CONCLUSIONS

As shown by Figs. 6 and 7, the experimental accuracy of the Planck Surveyor mission is effectively limited by astrophysical foregrounds. At high Galactic latitudes, however, fluctuations due to the Galactic dust, free-free and synchrotron emission, which are the main foreground components for angular scales $\gtrsim 30'$, are expected to be well below the primordial CMB anisotropies in several Planck channels. On these angular scales, i.e. for multipoles $\ell \lesssim 300$, foreground fluctuations are minimum at $\simeq 70$ GHz (see Figs. 8 and 9).

On smaller scales, the most troublesome foreground component are extragalactic sources. For wavelengths $\gtrsim 1$ mm, the dominant population is made of flat-spectrum and possibly of some inverted spectrum radio sources; estimates using very different methods indicate that their counts can be evaluated, at the fluxes relevant to estimate fluctuations in Planck channels, to better than a factor of 2 at frequencies up to at least 100 GHz. The uncertainty is larger for evolving dusty galaxies which are expected to dominate the counts at shorter wavelengths, but important constraints are set by SCUBA counts and by determinations of the extragalactic mm/sub-mm background spectrum. Point source fluctuations are larger than CMB anisotropies on very small angular scales ($\ell > 2000$, see Fig. 9). In the frequency region 100–200 GHz, however, their amplitude is significantly below the CMB signals for all scales accessible to Planck instruments.

Fluctuations due to clustering are generally small in comparison with Poisson fluctuations, at least in the case of radio sources (Fig. 10). Recent results indicating, in the case of evolving dusty galaxies, a clustering signal exceeding Poisson fluctuations, are likely to be rather extreme upper limits.

CMB polarization measurements are more challenging and the contamination by polarized foreground emissions has not been studied in depth. However, preliminary results suggest that the extraction of the CMB polarization is possible, with a signal to noise ratio > 3 , for $50 \lesssim \ell \lesssim 1000$.

On the other hand, the study of foregrounds is of great interest per se. Planck will carry out calibrated all-sky surveys at 9 frequencies between 30 and 860 GHz, covering an essentially unexplored spectral region. From several hundred to many thousands of sources can be detected as $\geq 5\sigma$ peaks at each frequency. More refined analyses, exploiting the different spectral properties and the different angular scales of sources in comparison with CMB fluctuations, may increase the number of detectable source by substantial factors.

Planck will provide the best calibrated all sky maps of the diffuse Galactic emissions (synchrotron, free-free and dust), of the Sunyaev-Zeldovich effect in clusters of galaxies and of extragalactic sources. It will extend the counts of the latter by about two orders of magnitude in flux. The information provided by Planck surveys will be unique: large area radio continuum surveys above 30 GHz are not feasible from the ground since the beam area of a given telescope scales as ν^{-2} .

Planck measurements will also determine the spectral energy distribution of bright sources over a factor $\simeq 30$ in frequency, covering a region where spectral features carrying essential information on physical conditions of sources show up (self-absorption turnovers of very compact components, high frequency flares, breaks due to energy losses of relativistic electrons, ...). While lower frequency surveys provide much more detailed information relevant to define *phenomenological* evolution properties, surveys at mm wavelengths are unique to provide information on the *physical* properties.

Planck will also provide the first complete samples of the extremely interesting classes of extragalactic radio sources characterized by inverted spectra (i.e. flux density increasing with frequency), which are very difficult to detect, and therefore are either missing from, or strongly underrepresented in low frequency surveys and may be very difficult to distinguish spectrally from fluctuations in the CBR [24].

Strongly inverted spectra up to tens of GHz can be produced in very compact, high electron density regions, by optically thick synchrotron emission or by free-free absorption. Examples are known also among galactic sources.

In conclusion, extragalactic sources will not be a threat to Planck's cosmological investigations. At the same time, Planck will provide extremely interesting data for astrophysical studies.

REFERENCES

1. Allen, S. W., and Fabian, A. C., *M.N.R.A.S.*, **297**, L57 (1998).
2. Aller, M.F., Aller, H.D., Hughes, P.A., and Latimer, G.E., *Ap. J.*, in press, astro-ph/9810485 (1998).
3. Altenhoff, W.J., Thum, C., and Wendker, H.J., *Astr. Ap.*, **281**, 161 (1994).
4. Arnaud, M., and Evrard, A.E. *M.N.R.A.S.*, preprint, astro-ph/9806353 (1998).
5. Bahcall, N.A., and Cen, R., *Ap. J.*, **407**, L49, (1993).
6. Atrio-Barandela, F., and Mücke, J.P., *Ap. J.*, in press, astro-ph/9811158 (1998).
7. Bahcall, N.A., and Chen, R., *Ap. J.*, **407**, L49 (1993).
8. Banday, A., and Wolfendale, A., *M.N.R.A.S.*, **245**, 182 (1990).
9. Bartlett, J.G., and Amram, P., in *Fundamental Parameters in Cosmology*, proc. Rencontres de Moriond, astro-ph/9804330 (1998).
10. Barbosa, D., Bartlett, J. G., Blanchard, A., and Oukbir, J., *Astr. Ap.*, **314**, 13 (1996).
11. Barvainis, R., and Lonsdale, C., *Astron. J.*, **115**, 885 (1998).
12. Berkhuijsen, E.M., Haslam, C.G.T., and Salter, C.J., *Astr. Ap.*, **14**, 252 (1971).
13. Birkinshaw, M., *Physics Reports*, preprint, astro-ph/9808050 (1998).
14. Bouchet, F.R., Prunet, S., and Sethi, S.K., *M.N.R.A.S.*, in press, astro-ph/9809353 (1999).
15. Burigana, C., and Popa, L., *Astr. Ap.*, **334**, 420 (1998).
16. Cavaliere, A., Danese, L., and De Zotti, G., *Ap. J.*, **217**, 6, (1977).
17. Cavaliere, A., Colafrancesco, S., and Menci, N., *Ap. J.*, **415**, 50 (1993).
18. Cavaliere, A., Menci, N., and Tozzi, P., *Ap. J.*, **484**, L21 (1997).
19. Cavaliere, A., Menci, N., and Tozzi, P., *Ap. J.*, **501**, 493 (1998).
20. Colafrancesco, S., and Vittorio, N., *Ap. J.*, **422**, 443 (1994).
21. Colafrancesco, S., Mazzotta, P., Rephaeli, Y., and Vittorio, N., *Ap. J.*, **479**, 1 (1997).
22. Cooray, A., preprint (1999).
23. Cox, P., Mezger, P.G., Sievers, A., Navarro, F., Bronfman, L., Kreysa, E., and Haslam, G., *Astr. Ap.*, **297**, 168 (1995).
24. Crawford, T., Marr, J., Partridge, R.B., and Strauss, M.A., *Ap. J.*, **460**, 225 (1996).
25. De Luca, A., Desert, F.X., and Puget, J.L., *Astr. Ap.*, **300**, 335 (1995).
26. Davies, R.D., Watson, R.A., and Gutierrez, C.M., *M.N.R.A.S.*, **278**, 925, (1996).

27. Davies, R.D., and Wilkinson, A., in *Fundamental Parameters in Cosmology*, proc. Rencontres de Moriond, astro-ph/9804208
28. Dennison, B., Simonetti, J.H., and Topasna, G.A., *Publ. Astron. Soc. Aust.*, **15**, 147 (1998).
29. de Oliveira-Costa, A., Kogut, A., Devlin, M.J., Netterfield, C.B., Page, L.A., and Wollack, E.J., *Ap. J.*, **482**, L17 (1997).
30. De Zotti, G., Toffolatti, L., and Granato, G.L., in *Fundamentals parameters in Cosmology*, proc. XXXIII Rencontres de Moriond, in press, astro-ph/9804004 (1998).
31. De Zotti, G., and Toffolatti, L., *Ap. Lett. Comm.*, in press, astro-ph/9812069 (1998).
32. Di Matteo, T., and Fabian, A.C., *M.N.R.A.S.*, **286**, L50 (1997).
33. Draine, B.T., and Lazarian, A., *Ap. J.*, **494**, L19, (1998).
34. Draine, B.T., and Lazarian, A., *Ap. J.*, in press, astro-ph/9807009 (1999).
35. Duncan, A.R., Stewart, R.T., Haynes, R.F., and Jones, K.L., *M.N.R.A.S.*, **277**, 36 (1995).
36. Ekart, A., and Genzel, R., *M.N.R.A.S.*, **284**, 576 (1997).
37. Eke, V. R., Cole, S., and Frenk, C. S., *M.N.R.A.S.*, **282**, 263 (1996).
38. Eke, V. R., Cole, S., Frenk, C. S., and Patrick Henry, J., *M.N.R.A.S.*, **298**, 1145 (1998).
39. Evrard, A.E., In: Fitchett M., Oegerle W. (eds.) *Clusters of Galaxies*. Cambridge University Press, Cambridge (1990).
40. Evrard, A.E., Henry, J.P., *Ap. J.*, **383**, 95 (1991).
41. Fabian, A. C., Crawford, C. S., Edge, A. C., and Mushotzky, R. F., *M.N.R.A.S.*, **267**, 779 (1994).
42. Fabian, A.C., and Rees, M.J., *M.N.R.A.S.*, **277**, L55 (1995).
43. Fanti, C., Fanti, R., Dallacasa, D., Schilizzi, R.T., Spencer, R.E., and Stanghellini, C., *Astr. Ap.*, **302**, 317 (1995).
44. Fixsen, D.J., Dwek, E., Mather, J.C., Bennett, C.L. and Shafer, R.A., *Ap. J.*, **508**, 123, (1998).
45. Gaustad, J., McCullough, P., and van Buren, D., *P.A.S.P.*, **108**, 351 (1996).
46. Gaustad, J., Rosing, W., Chen, G., McCullough, P., and van Buren, D., *A.A.S. Meeting*, **190**, #30.05 (1997).
47. Gautier, T.N., Boulanger, F., Perault, M., and Puget, J.-L., *Astron. J.*, **103**, 1313 (1992).
48. Ginzburg, V.L., and Syrovatskii, S.I., *Origin of Cosmic Rays*, New York: Pergamon Press (1964).
49. Griffin, M., et al., *SPIRE. A Bolometer Instrument for FIRST. A Proposal Submitted to ESA.* (1998).
50. Guiderdoni, B., Hivon, E., Bouchet, F.R., and Maffei, B., *M.N.R.A.S.*, **295**, 877 (1998).
51. Gutierrez, C.M., et al., *Ap. J.*, **442**, 10 (1995).
52. Haffner, L.M., Reynolds, R.J., and Tufte, S.L., *Ap. J.*, **501**, L83 (1998).
53. Hancock, S., et al., *M.N.R.A.S.*, **289**, 505 (1997).
54. Haslam, C.G.T., Klein, U., Salter, C.J., Stoffel, H., Wilson, W.E., Cleary, M.N., Cooke, D.J., and Thomasson, P., *Astr. Ap.*, **100**, 209 (1982).
55. Hauser, M.G., et al., *Ap. J.*, **508**, 25 (1998).
56. Hildebrand, R.H., Dragovan, M., *Ap. J.*, **450**, 663, (1995).
57. Henry, J.P., and Arnaud, K.A., *Ap. J.*, **372**, 410 (1991).
58. Henry, J.P., *Ap. J.*, **489**, L1 (1997).
59. Hobson, M.P., Barreiro, R.B., Toffolatti, L., Lasenby, A.N., Sanz, J.L., Jones, A.W., and Bouchet, F.R., *M.N.R.A.S.*, in press, astro-ph/9810241 (1998).
60. Hobson, M. P., Jones, A. W., Lasenby, A. N., and Bouchet, F.R., *M.N.R.A.S.*, **300**, 1 (1998).
61. Holdaway, M.A., Owen, F.N., and Rupen, M.P., *NRAO report*, unpublished (1994).
62. Ivison, R.J., Hughes, D.H., and Bode, M.F., *M.N.R.A.S.*, **257**, 47 (1992).
63. Jonas, J.L., Baart, E.E., and Nicolson, G.D., *M.N.R.A.S.*, **297**, 977 (1998).
64. Kaiser, N., *Ap. J.*, **383**, 104 (1991).
65. Keating, B., Timbie, P., Polnarev, A., and Steinberger, J., *Ap. J.*, **495**, 580 (1998).
66. Knapp, G.R., Bowers, P.F., Young, K., and Phillips, T.G., *Ap. J.*, **455**, 293 (1995).
67. Knapp, G.R., and Patten, B.M., *Astron. J.*, **101**, 1609, (1991).
68. Kogut, A., Banday, A.J., Bennett, C.L., Górski, K.M., Hinshaw, G., and Reach, W.T., *Ap. J.* **460**, 1 (1996).
69. Kompaneets, A.S., *Sov. Phys. JETP*, **4**, 730 (1957).
70. Kowalski, M.P., Ulmer, M.P., Cruddace, R.G., and Wood, K.S., *Ap. J. Suppl.*, **56**, 403 (1984).
71. Lasenby, A.N., in *Microwave Background Anisotropies*, proc. XVI Moriond Astrophysics Meeting, eds. F.R. Bouchet, R. Gispert, B. Guiderdoni, J. Trân Thanh Vân, p. 453 (1996).
72. Lawson, K.D., Mayer, C.J., Osborn, J.L., and Parkinson, M.L., *M.N.R.A.S.*, **225**, 307 (1987).
73. Lee, H.M., and Draine, B.T., *Ap. J.*, **290**, 211 (1985).
74. Leitch, E., Readhead, A.C.S., Pearson, T.J., and Myers, S.T., *Ap. J.*, **486**, L23 (1997).
75. Le Roux, E., *Ann. Astroph.*, **24**, 71 (1961).
76. Loan, A.J., Wall, J.V., and Lahav, O., *M.N.R.A.S.*, **286**, 994 (1997).
77. Longair, M., *High energy astrophysics*, Cambridge: Cambridge Un. Press (1994).
78. Magliocchetti, M., Maddox, S.J., Lahav, O., and Wall, J.V., *M.N.R.A.S.*, in press, astro-ph/9806342 (1998).

79. Marcelin, M., Amram, P., Bartlett, J.G., Valls-Gabaud, D., and Blanchard, A., *Astr. Ap.*, **338**, 1 (1998).
80. Markevitch, M., *Ap. J.*, **504**, 27 (1998).
81. Mazzotta, P., Ph.D. Thesis University of Roma “Tor Vergata” (1999).
82. Melhuish, S.J., et al., *M.N.R.A.S.*, **286**, 48 (1997).
83. Mushotzky, R.F., Scharf, C.A., *Ap. J.*, **482**, L13 (1997).
84. Narayan, R., Mahadevan, R., Grindlay, J.E., Popham, R.G., and Gammie, C., *Ap. J.*, **492**, 554 (1998).
85. Narayan, R., and Yi, I., *Ap. J.*, **444**, 231 (1995).
86. Nartallo, R., Gear, W.K., Murray, A.G., Robson, E.I., Hough, J.H., *M.N.R.A.S.*, **297**, 667 (1998).
87. Nishimura, J., et al. *Proceedings 21st ICRC*, vol. 3, p. 213 (1991).
88. O’Dea, C.P., and Baum, S.A., *Astron. J.*, **113**, 148 (1997).
89. Pallavicini, R., and White, S.M., in *Science with Large Millimetre Arrays*, P.A. Shaver ed., Berlin: Springer, p. 268 (1996).
90. Peebles, P.J.E., *The Large-Scale Structure of the Universe*, Princeton: Princeton University Press, 1980.
91. Platania, P., Bensadoun, M., Bersanelli, M., De Amici, G., Kogut, A., Levin, S., Maino, D., and Smoot, G.F., *Ap. J.*, **505**, 473 (1998).
92. Press, W.H., and Schechter, P., *Ap. J.*, 187, 425 (1974).
93. Puget, J.-L., Abergel, A., Bernard, J.-P., Boulanger, F., Burton, W.B., Désert, F.-X., and Hartmann, D., *Astr. Ap.*, **308**, 5 (1996).
94. Prunet, S., Sethi, S.K., Bouchet, F.R., and Miville-Deschênes, M.-A., *Astr. Ap.*, **339**, 187 (1998).
95. Readhead, A.C.S., Taylor, G.B., Pearson, T.J., and Wilkinson, P.N., *Ap. J.*, **460**, 634 (1996).
96. Reich, P., and Reich, W., *Astr. Ap. Suppl.*, **63**, 205 (1986).
97. Reichart, D.E., Castander, F.J., Nichol, R.C., *Ap. J.*, in press, astro-ph/9810487 (1998).
98. Reynolds, R.J., in *The Galactic and Extragalactic Background Radiation*, eds. S. Bowyer and C. Leinert, p. 157 (1990).
99. Reynolds, R.J., *Ap. J.*, **392**, L35 (1992).
100. Reynolds, R.J., Tufte, S.L., Haffner, L.M., Jaehnig, K., and Percival, J.W., *Publ. Astron. Soc. Aust.*, **15**, 14 (1998).
101. Rowan-Robinson, M., and Pearson, C., in *Science with Large Millimetre Arrays*, P.A. Shaver ed., Berlin: Springer, p. 61 (1996).
102. Rybicki, G.B., and Lightman, A.P., *Radiative Processes in Astrophysics*, New York: Wiley, 1979.
103. Sadat, R., Blanchard, A., and Oukbir, J., *Astr. Ap.*, **329**, 21 (1998).
104. Schlegel, D.J., Finkbeiner, D.P., and Davis, M., *Ap. J.*, **500**, 525 (1998).
105. Scott, D., and White, M., 1999, *Astr. Ap.*, submitted, astro-ph/9808003.
106. Seaquist, E.R., and Taylor, A.R., *Ap.J.*, **387**, 624, (1992).
107. Simonetti, J.H., Dennison, B., and Topasna, G.A., *Ap. J.*, **458**, L1 (1996).
108. Sivan, J.P., *Astr. Ap. Suppl.*, **16**, 163 (1974).
109. Smail, I., Ivison, R.I., and Blain, A.W., *Ap. J.*, **490**, L5 (1997).
110. Smoot, G.F., preprint astro-ph/9801121 (1998).
111. Sokasian, A., Gawiser, E., and Smoot, G.F., *Ap. J.*, submitted, astro-ph/9811311 (1998).
112. Sunyaev, R.A., and Zel’dovich, Y.B., *Astrophys. Sp. Sci.*, **7**, 3 (1970).
113. Tegmark, M., and de Oliveira-Costa, A., *Ap. J.*, **500**, L83 (1998).
114. Tegmark, M., and Efstathiou, G., *M.N.R.A.S.*, **281**, 1297 (1996).
115. Toffolatti, L., Argüeso-Gómez, F., De Zotti, G., Mazzei, P., Franceschini, A., Danese, L., Burigana, C., *M.N.R.A.S.*, **297**, 117 (1998).
116. van Breugel, W., Miley, G., and Heckman, T., *Astron. J.*, **89**, 5 (1984).
117. Veeraraghavan, S., and Davies, R.D., in *Particle Physics and the Early Universe*, eds. Batel, R., Jones, M.E., and Green, D.A. (1997).
118. Viana, P.T.P., Liddle, A.R., astro-ph/9803244 (1998).
119. Webber, W., in *Composition and origin of cosmic rays*, Shapiro ed., Dordrecht: Reidel (1983).
120. Weiler, K.W., and Sramek, R.A., *Ann. Rev. Astr. Ap.*, **26**, 295 (1988).
121. Weiner, B.J., and Williams, T.B., *Astron. J.*, **111**, 1156 (1996).
122. Wright, E.L., *Ap. J.*, **496**, 1 (1998).